Comput Mech (2010) 46:399–415
DOI 10.1007/s00466-010-0481-5

ORIGINAL PAPER

High-speed impact of electromagnetically sensitive fabric and induced projectile spin

T. I. Zohdi

Received: 19 August 2009 / Accepted: 3 February 2010 / Published online: 9 March 2010
© Springer-Verlag 2010

Abstract This work deals with the dynamic contact of a rigid body with a deformable electromagnetically sensitive fabric structure, represented by a network model. Of particular interest are the electromagnetically induced forces generated on the fabric, which are proportional to the external electric field ($\boldsymbol{E}^{EXT}$) and the velocity crossed with the external magnetic field ($\boldsymbol{v} \times \boldsymbol{B}^{EXT}$). These forces transmit reactions to the rigid contacting object, which can induce rotational motion. Modeling and simulation of this effect can be useful in ballistic shielding applications, because the rotation of an incoming, ogival, projectile allows it to be more easily impeded. A modular formulation for the deformation of impacted fabric structures, represented by a network model, is developed in this paper, characterized by (1) stretching of interconnected yarn networks, described by simple constitutive relations, including yarn damage, (2) interaction with impacting objects, incorporating contact with friction and (3) electromagnetic sensitivity and actuation, demonstrating how the Lorentz force can be harnessed to break symmetric deformation patterns in order to induce spin onto an incoming object, whether that object is electromagnetically sensitive or not.

Keywords Fabric networks · Electromagnetics · Impact

T. I. Zohdi (✉)
Department of Mechanical Engineering, University of California, 6195 Etcheverry Hall, Berkeley, CA 94720-1740, USA
e-mail: zohdi@me.berkeley.edu

1 Introduction

The focus of this paper is to model and simulate the deformation of an electromagnetically sensitive fabric structure, represented by a network model, that is induced via high-speed contact with a rigid object. An effect of interest is the strongly asymmetric deformation arising from the Lorentz force, and its utilization to induce the rotation (via contact forces) of an incoming object. To explain the effect clearly, we will consider a flat planar sheet of electromagnetically sensitive fabric (Fig. 1) placed directly in front of an external electromagnetic field. Afterward, we then consider the impact of a rigid body against the fabric, which thrusts the system into the electromagnetic field. The electromagnetic field induces forces that are proportional to external electric field $\boldsymbol{E}^{EXT}$ and the velocity crossed with the external magnetic field ($\boldsymbol{v} \times \boldsymbol{B}^{EXT}$) onto the fabric, which in turn, due to normal contact and friction forces, induces reactions onto the contacting object, which can cause it to rotate. This rotation occurs even if the rigid object is not electromagnetically sensitive, due to the reaction forces produced by the fabric, which is electromagnetically sensitive. As mentioned, an application of interest is to induce enough spin to sufficiently rotate an incoming ogival object (a projectile), so that it can be more easily stopped.[1] In this case, we emphasize that the field would not have to be strong enough to stop the projectile, only strong enough to make it tilt. The sensitivity of the fabric to electromagnetic fields can be induced by seeding small-scale (nano) particles within the weave (Fig. 2), which

[1] Generally, tumbling helps to impede an ogival projectile, since the projectile will project a larger contact area onto the fabric. Induced tumbling of projectiles has been attempted for many years by non-electromagnetic means (see Meyers [24] for reviews).

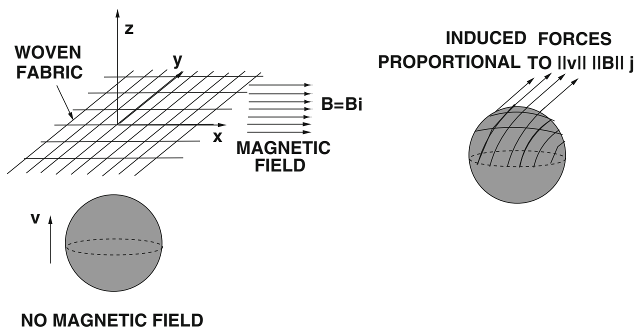

Fig. 1 An electromagnetically-sensitive fabric being "pushed" into a magnetic field by a projectile. The velocity of the object and the magnetic field induce forces proportional to the velocity attained by the fabric and the external magnetic field magnitude

is a relatively standard approach to produce electromagnetically sensitive polymers.

Remarks There exist a wide range of applications for ballistic fabric shields, such as body armor and shielding of critical military and commercial structural components. The reader is referred to Godfrey and Rossettos [13], Rossettos and Godfrey [30], Roylance and Wang [31], Taylor and Vinson [39], Shim et al. [33], Johnson et al. [18], Tabiei and Jiang [36], Kollegal and Sridharan [19], Walker [42], Cheeseman and Bogetti [7], Duan et al. [9–11] Kwong and Goldsmith [20], Lim et al [22,23], Shockey et al [34], Tan et al [38], Verzemnieks [41], Zohdi [44], Zohdi and Steigmann [45], Zohdi [51], Zohdi and Powell [49] and Powell and Zohdi [29] for a cross-sectional view of the field. For an exhaustive and comprehensive overview of all aspects of ballistic fabric, see Tabiei and Nilakantan [37]. To the knowledge of the author, no works have explored the deformation of electromagnetically sensitive fabric shielding.

2 Reduced order fabric network model

2.1 Overall model

We consider an undeformed, initially planar, network representation of a woven fabric of yarn (Fig. 2). The main ingredients of this reduced order model are:

- The yarn are joined at the nodes, in other words, they are sutured together at those locations to form a network connected by pin-joints (nodes) (Fig. 2). In reality the yarn are tightly woven and the nodes are the criss-cross contact junctions between the warp and the fill of the weave.
- The mass of the fabric is lumped to coincide with the pin-joint locations. The deformation of the fabric is dictated by solving a coupled system of differential equations of motion for the interconnected lumped masses.

2.2 Lumped mass representation

For each lumped mass, dynamic motion is computed via

$$m_i \ddot{\boldsymbol{r}}_i = \underbrace{\boldsymbol{\psi}_i^{tot}}_{total} = \underbrace{\boldsymbol{\psi}_i^{con}}_{\text{contact forces}} + \underbrace{\boldsymbol{\psi}_i^{fric}}_{\text{friction forces}} + \underbrace{\boldsymbol{\psi}_i^{em}}_{\text{electromagnetic forces}} + \underbrace{\sum_{I=1}^{4} \boldsymbol{\psi}_{iI}^{yarn}}_{\text{surrounding yarn}}, \tag{2.1}$$

where $i = 1, 2, \ldots, N$, N being the number of lumped masses (nodes), $\boldsymbol{\psi}_i^{con}$ represents the (normal) contact force contribution to node i, $\boldsymbol{\psi}_i^{fric}$ represents the friction (contact) force contribution, $\boldsymbol{\psi}_i^{em}$ represents the electromagnetic contribution, $\boldsymbol{\psi}_{iI}^{yarn}$ represents the axial contributions of the four yarn intersecting at node i (Fig. 1) and where m_i is the mass of a single lumped mass node, i.e. the total fabric mass divided by the total number of nodes.

2.3 Yarn forces

We assume that the compressive response of the fabric is of insignificant interest for the applications under consideration, and employ a so-called relaxed model, whereby a zero stress state is enforced for any compressive strains. For details on a wide variety of relaxed models, we refer the reader to works dating back to Pipkin [27], in the context of wrinkling sheets, Buchholdt et al. [3], Pangiotopoulos [25], Bufler and Nguyen-Tuong [4] and Cannarozzi [5,6], Steigmann [35], Haseganu and Steigmann [14,15] and [16], Atai and Steigmann [1,2] for applications to elastostatic analysis of structural fabric and Papadrakakis [26] for related, general, pseudo dynamic relaxation methods. Relaxed formulations have served as a foundation for more elaborate models describing rupture of ballistic fabric shielding in Zohdi [44], Zohdi and Steigmann [45], Zohdi [51] and Zohdi and Powell [49], and are the basis for the present approach. We make the following simplifying assumptions:

- the yarn are quite thin, therefore one may assume a uniaxial-stress type condition,
- the joint connections produce no bending or moments,
- the yarn buckling is ignored,
- the forces only act along the length of the yarn and
- the bars remain straight, undergoing a homogeneous stress state.

We typically write constitutive laws in terms of the Piola-stresses. Mimicing 3-D approaches, we first define the first-Piola stress Kirchhoff stress:

$$P = \frac{\text{force on referential area}}{\text{referential area}}, \tag{2.2}$$

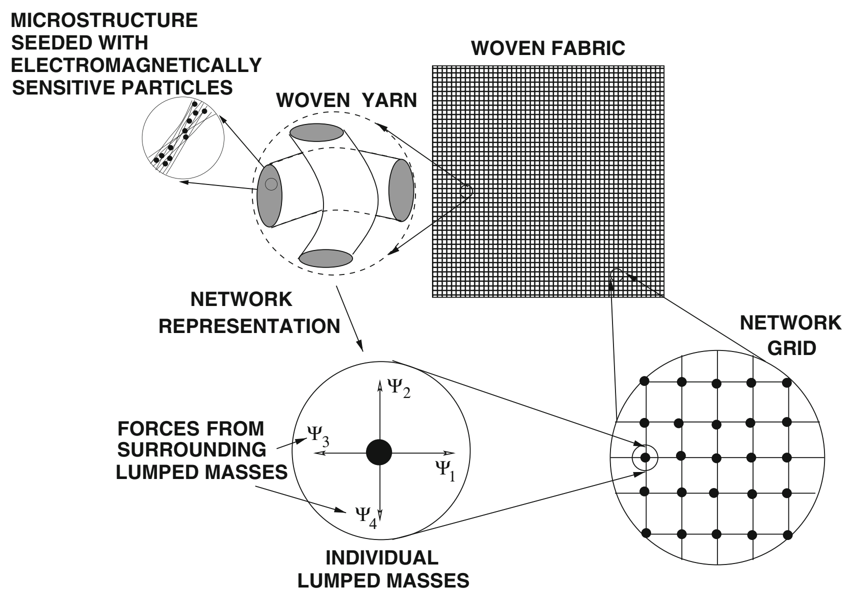

Fig. 2 A network representation of woven-fabric. The yarn are joined at the nodes, in other words, they are sutured together at those locations to form a network connected by pin-joints, and the mass and electrical charge of the material are lumped at the suture points

and then transform the result to the the second Piola stress via $P = FS$, in order to symmetrize it, although in 1-D this is superfluous. One can then employ a standard constitutive relation $S = \mathcal{F}(U)$. One primary objective is to extract the force ($\boldsymbol{\psi}^{yarn}$), therefore

$$P = \frac{\psi^{yarn}}{A_o} \Rightarrow \psi^{yarn} = USA_o = \frac{L}{L_o}SA_o. \tag{2.3}$$

The axial strains, for structural fabric, such as Zylon or Kevlar, are expected to be in the range of 2–10% before rupturing.[2] Therefore, a relatively simple Kirchhoff-St. Venant material model is reasonable. The stored energy is $W = \frac{1}{2}\mathbb{E}E^2$, $\mathbb{E}$ is Young's modulus, $E \stackrel{\text{def}}{=} \frac{1}{2}(U^2 - 1)$ is the Green-Lagrange strain, $U = \frac{L}{L_o}$ is the stretch ratio, L is the deformed length of the yarn and L_o is its original length. The second Piola–Kirchhoff stress is given by $\frac{\partial W}{\partial E} = S = \mathbb{E}E$, thus

$$\psi^{yarn} = \frac{L}{L_o}SA_o = \frac{L}{L_o}\left(\mathbb{E}\frac{U^2-1}{2}\right)A_o. \tag{2.4}$$

The forces from the Ith surrounding yarn segment (there are four of them for the type of weaving pattern considered) acting on the ith lumped mass is $\boldsymbol{\psi}^{yarn}_{iI} = U_I S_I A_o \boldsymbol{a}_{iI}$ (A_o is the undeformed cross-sectional area of the yarn), where the unit axial yarn direction is given by $\boldsymbol{a}_{iI} = \frac{\boldsymbol{r}_I^+ - \boldsymbol{r}_I^-}{||\boldsymbol{r}_I^+ - \boldsymbol{r}_I^-||}$, where $\boldsymbol{r}_I^+$ denotes the endpoint connected to the lumped mass and $\boldsymbol{r}_I^-$ denotes the endpoint that is not connected to the lumped mass (Fig. 1).[3] Clearly, $\boldsymbol{\psi}^{yarn}_{iI}$ is a function of the nodal positions ($\boldsymbol{r}_i$), which are all coupled together, leading to a system of equations. In order to solve the resulting coupled system, we develop an iterative solution scheme later in the presentation.

2.4 Yarn damage

Generally, the microstructure of the yarn is composed of microscale fibrils. This is the case with materials such as Zylon, which is a polymeric material produced by the Toyobo Corporation (Toyobo [40]), Kevlar or other aramid-based materials. For example, Zylon has a multiscale structure constructed from PBO (Polybenzoxale) microscale fibrils, which are bundled together to form yarn, which are then tightly woven into sheets. For Zylon, each yarn contains approximately 350 microfibrils, which are randomly misaligned within the yarn, leading to a gradual type of failure, since the microfibrils become stretched to different lengths (within the yarn), when the yarn is in tension. The simplest approach to describe failure of a yarn is to check whether a critical stretch has been attained, $U(t) \geq U_{crit}$, and to track the progressive damage for a yarn with a single damage (isotropic) variable, $0 \leq \alpha \leq 1$, used in the representation

$$S = \alpha\mathbb{E}E. \tag{2.5}$$

The damage variable for a yarn segment I, $\alpha_I = \mathcal{F}(U_I)$ represents the fraction of microfibrils that are *not ruptured*, within the Ith yarn.[4] Thus, for a yarn that is undamaged, $\alpha_I = 1$, while for a yarn that is completely damaged, $\alpha_I = 0$. A particularly simple damage representation is (Zohdi and Powell [49])

[2] For example, Zylon ruptures at approximately a 3% axial strain (Toyobo [40]).

[3] $||\cdot||$ indicates the Euclidean norm in R^3.

[4] This topic, which is relevant in a multiscale setting, has been explored in depth in Zohdi and Steigmann [45] and Zohdi and Powell [49], Powell and Zohdi [29].

$$\alpha_I(t) = min\left(\alpha_I(0 \le t^* < t), e^{\left(-\lambda\left(\frac{U(t)-U_{crit}}{U_{crit}}\right)\right)}\right), \tag{2.6}$$

where $\alpha_I(U(t=0)) = 1$, $U(t)$ is the stretch of the yarn at time t, and where $0 \le \lambda$ is a damage decay parameter. The above relation indicates that damage is irreversible, i.e. α_I is a monotonically decreasing function. As $\lambda \to \infty$, the type of failure tends towards sudden rupture, while as $\lambda \to 0$, then there is no damage generated.

2.5 Electromagnetic "lumping"

In order to introduce the electromagnetic sensitivity into the fabric model, recall the main observations in conjunction with electromagnetic phenomena, namely (a) if a point charge q experiences a force $\boldsymbol{F}_e$, the electric field, $\boldsymbol{E}$, at a position of the charge is defined by $\boldsymbol{F}_e = q\boldsymbol{E}$, (b) if the charge is moving, another force may arise, $\boldsymbol{F}_m$, which is proportional to its velocity $\boldsymbol{v}$, and which is denoted as the "magnetic induction" (induced) or just the "magnetic field", $\boldsymbol{B}$, such that $\boldsymbol{F}_m = q\boldsymbol{v} \times \boldsymbol{B}$ and (c) if the forces occur concurrently (the charge is moving through the region possessing both electric and magnetic fields), then $\boldsymbol{F} = q\boldsymbol{E} + q\boldsymbol{v} \times \boldsymbol{B}$. Consistent with the inertial lumped mass approximations, the electromagnetic lumped mass nodes in fabric experience electromagnetic forces of the form

$$\boldsymbol{\psi}_i^{em} = q_i\left(\boldsymbol{E}^{EXT} + \boldsymbol{v}_i \times \boldsymbol{B}^{EXT}\right), \tag{2.7}$$

where q_i is the charge of the lumped mass and $\boldsymbol{E}^{EXT}$ and $\boldsymbol{B}^{EXT}$ are the external fields.

Note: $\boldsymbol{E}^{EXT}$ and $\boldsymbol{B}^{EXT}$ can be considered as static (or extremely slowly-varying), and thus uncoupled and independently controllable. We assume that the fields are independent of the response of the system (dead loading), and that the electromagnetic interaction between particles is negligible. For a review of extensive work on nodal and charged particle interaction, see Zohdi [46–53].

3 Iterative solution schemes

3.1 General time-stepping schemes

In order describe the overall time-stepping scheme, we first start with the dynamics of a single (ith) lumped mass. The equation of motion is given by

$$m_i\dot{\boldsymbol{v}}_i = \boldsymbol{\psi}_i^{tot}, \tag{3.1}$$

where $\boldsymbol{\psi}_i^{tot}$ is the total force provided from interactions with the external environment (yarn, electromagnetics, etc). Employing the trapezoidal-like rule ($0 \le \phi \le 1$)[5]

$$\boldsymbol{r}_i(t+\Delta t) = \boldsymbol{r}_i(t) + \boldsymbol{v}_i(t)\Delta t + \frac{\phi(\Delta t)^2}{m_i}\left(\phi\boldsymbol{\psi}_i^{tot}(\boldsymbol{r}_i(t+\Delta t)) + (1-\phi)\boldsymbol{\psi}_i^{tot}(\boldsymbol{r}_i(t))\right) + \hat{\mathcal{O}}(\Delta t)^2, \tag{3.2}$$

where if $\phi = 1$, then Eq. 3.2 becomes the (implicit) Backward Euler scheme, which is very stable, dissipative and $\hat{\mathcal{O}}(\Delta t)^2 = \mathcal{O}(\Delta t)^2$ locally in time, if $\phi = 0$, then Eq. 3.2 becomes the (explicit) Forward Euler scheme, which is conditionally stable and $\hat{\mathcal{O}}(\Delta t)^2 = \mathcal{O}(\Delta t)^2$ locally in time and if $\phi = 0.5$, then Eq. 3.2 becomes the (implicit) Midpoint scheme, which is stable and $\hat{\mathcal{O}}(\Delta t)^2 = \mathcal{O}(\Delta t)^3$ locally in time. In summary, we have for the velocity.[6] Equation 3.2 can be solved recursively by recasting the relation as

$$\boldsymbol{r}_i^{L+1,K} = \mathcal{G}(\boldsymbol{r}_i^{L+1,K-1}) + \mathcal{R}_i, \tag{3.3}$$

where $K = 1, 2, 3, \ldots$ is the index of iteration within time step $L+1$ and $\mathcal{R}_i$ is a remainder term that does not depend on the solution, i.e. $\mathcal{R}_i \neq \mathcal{R}_i(\boldsymbol{r}_1^{L+1}, \boldsymbol{r}_2^{L+1} \ldots \boldsymbol{r}_N^{L+1})$. The convergence of such a scheme is dependent on the behavior of $\mathcal{G}$. Namely, a sufficient condition for convergence is that $\mathcal{G}$ is a contraction mapping for all $\boldsymbol{r}_i^{L+1,K}$, $K = 1, 2, 3\ldots$ In order to investigate this further, we define the iteration error as

$$\varpi_i^{L+1,K} \stackrel{\text{def}}{=} \boldsymbol{r}_i^{L+1,K} - \boldsymbol{r}_i^{L+1}. \tag{3.4}$$

A necessary restriction for convergence is iterative self consistency, i.e. the "exact" (discretized) solution must be represented by the scheme

$$\mathcal{G}(\boldsymbol{r}_i^{L+1}) + \mathcal{R}_i = \boldsymbol{r}_i^{L+1}. \tag{3.5}$$

Enforcing this restriction, a sufficient condition for convergence is the existence of a contraction mapping

$$||\underbrace{\boldsymbol{r}_i^{L+1,K} - \boldsymbol{r}_i^{L+1}}_{\varpi_i^{L+1,K}}|| = ||\mathcal{G}(\boldsymbol{r}_i^{L+1,K-1}) - \mathcal{G}(\boldsymbol{r}_i^{L+1})|| \le \eta^{L+1,K}||\boldsymbol{r}_i^{L+1,K-1} - \boldsymbol{r}_i^{L+1}||,$$

where, if $0 \le \eta^{L+1,K} < 1$ for each iteration K, then $\varpi_i^{L+1,K} \to \boldsymbol{0}$ for any arbitrary starting value $\boldsymbol{r}_i^{L+1,K=0}$, as $K \to \infty$. This type of contraction condition is sufficient, but

[5] See the Appendix 1 for a derivation.

[6] In order to streamline the notation, we drop the cumbersome $\mathcal{O}(\Delta t)$-type terms.

not necessary, for convergence. Explicitly, the recursion is

$$\boldsymbol{r}_i^{L+1,K} = \underbrace{\boldsymbol{r}_i^L + \boldsymbol{v}_i^L \Delta t + \frac{\phi(\Delta t)^2}{m_i}\left((1-\phi)\boldsymbol{\psi}_i^{tot,L}\right)}_{\mathcal{R}_i} + \underbrace{\frac{\phi(\Delta t)^2}{m_i}\left(\phi \boldsymbol{\psi}_i^{tot,L+1,K-1}\right)}_{\mathcal{G}(\boldsymbol{r}_i^{L+1,K-1})} \tag{3.6}$$

where

$$\boldsymbol{\psi}_i^{tot,L} = \boldsymbol{\psi}_i^{tot,L}(\boldsymbol{r}_1^L, \boldsymbol{r}_2^L \ldots \boldsymbol{r}_N^L) \tag{3.7}$$

and

$$\boldsymbol{\psi}_i^{tot,L+1,K-1} = \boldsymbol{\psi}_i^{tot,L+1,K-1}(\boldsymbol{r}_1^{L+1,K-1}, \boldsymbol{r}_2^{L+1,K-1} \ldots \boldsymbol{r}_N^{L+1,K-1}). \tag{3.8}$$

According to Equation, convergence is scaled by $\eta \propto \frac{(\Delta t)^2}{m_i}$, and that the contraction constant of $\mathcal{G}$ is (1) directly dependent on the magnitude of the interaction forces, (2) inversely proportional to the lumped masses m_i and (3) directly proportional to Δt. Thus, if convergence is slow within a time step, the time step size, which is adjustable, can be reduced by an appropriate amount to increase the rate of convergence. It is also desirable to simultaneously maximize the time-step sizes to decrease overall computing time, while obeying an error tolerance on the numerical solution's accuracy. In order to achieve this goal, we follow an approach found in Zohdi [46–53], originally developed for continuum thermo-chemical multifield problems where (1) one approximates $\eta^{L+1,K} \approx S(\Delta t)^p$ (S is assumed a constant) and (2) one assumes that the error within an iteration to behave according to $(S(\Delta t)^p)^K \varpi^{L+1,0} = \varpi^{L+1,K}$, $K = 1, 2, \ldots$, where $\varpi^{L+1,0}$ is the initial norm of the iterative error and S is intrinsic to the system.[7] The objective is to meet an error tolerance in exactly a preset number of iterations. To this end, one writes $(S(\Delta t_{\text{tol}})^p)^{K_d} \varpi^{L+1,0} = TOL$, where TOL is a tolerance and where K_d is the number of desired iterations.[8] If the error tolerance is not met in the desired number of iterations, the contraction constant $\eta^{L+1,K}$ is too large. Accordingly, one can solve for a new smaller step size, under the assumption that S is constant,

$$\Delta t_{\text{tol}} = \Delta t \left(\frac{\left(\frac{TOL}{\varpi^{L+1,0}}\right)^{\frac{1}{pK_d}}}{\left(\frac{\varpi^{L+1,K}}{\varpi^{L+1,0}}\right)^{\frac{1}{pK}}} \right). \tag{3.9}$$

[7] For the class of problems under consideration, due to the quadratic dependency on Δt, $p \approx 2$.

[8] Typically, K_d is chosen to be between five to ten iterations.

The assumption that S is constant is not crucial, since the time steps are to be recursively refined and unrefined throughout the simulation. The expression in Eq. 3.9 can also be used for time step enlargement, to reduce computational effort, if convergence is met in less than K_d iterations. Numerous parameter studies of this algorithm can be found in Zohdi [46–53]. An implementation of the procedure is as follows:

(1) GLOBAL FIXED – POINT ITERATION :
(SET i = 1 AND K = 0) :
(2) IF i > N THEN GO TO (4) (N = # OF NODES)
(3) IF i ≤ N THEN :
(a) COMPUTE MASS POSITION : $\boldsymbol{r}_i^{L+1,K}$
(b) ENFORCE CONTACT IF NECESSARY (DISCUSSED IN NEXT SECTION)
(c) GO TO (2) AND NEXT MASS (i = i + 1)
(4) COMPUTE/UPDATE FORCES $\boldsymbol{\psi}_i^{tot,K}$ AND YARN DAMAGE : α_I
(5) ERROR MEASURE :
(a) $\varpi_K \stackrel{\text{def}}{=} \frac{\sum_{i=1}^N ||\boldsymbol{r}_i^{L+1,K} - \boldsymbol{r}_i^{L+1,K-1}||}{\sum_{i=1}^N ||\boldsymbol{r}_i^{L+1,K} - \boldsymbol{r}_i^{L}||}$ (normalized)
(b) $Z_K \stackrel{\text{def}}{=} \frac{\varpi_K}{TOL_r}$
(c) $\Phi_K \stackrel{\text{def}}{=} \left(\frac{\left(\frac{TOL}{\varpi_0}\right)^{\frac{1}{pK_d}}}{\left(\frac{\varpi_K}{\varpi_0}\right)^{\frac{1}{pK}}} \right)$
(6) IF TOLERANCE MET ($Z_K \le 1$) AND $K < K_d$ THEN :
(a) CONSTRUCT NEW TIME STEP : $\Delta t = \Phi_K \Delta t$
(b) SELECT MINIMUM : $\Delta t = MIN(\Delta t^{lim}, \Delta t)$
(c) INCREMENT TIME : $t = t + \Delta t$ AND GO TO (1)
(7) IF TOLERANCE NOT MET ($Z_K > 1$) AND $K = K_d$ THEN :
(a) CONSTRUCT NEW TIME STEP : $\Delta t = \Phi_K \Delta t$
(b) RESTART AT TIME = t AND GO TO (1)

(3.10)

4 Fabric/rigid-body interaction

Following classical contact algorithms, if penetration of a fabric node into the projectile is detected ("contact"), the following process is enacted: (1) Move the fabric node to the closest point on the rigid body's surface [Note: there are a variety of algorithms to perform this operation (see Wriggers [43] for details)] and (2) If there is friction, then a stick condition is assumed (assuming a common position and velocity for the point on the surface of the projectile and the fabric node). The friction force is then checked against the static limit, which if violated, enacts a sliding friction force.

4.1 Details

Assuming interpenetration for a node i, we calculate the contact force on a node i (Fig. 3)

$$\boldsymbol{\psi}_i^{con} = \frac{m_i}{\Delta t^2}(\boldsymbol{r}_i^{f,corr}(t+\Delta t) - \boldsymbol{r}_i^{f,pred}(t+\Delta t)) \tag{4.1}$$

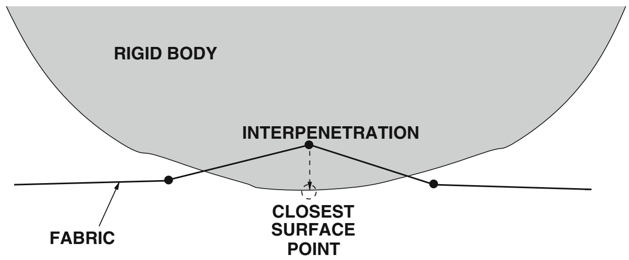

Fig. 3 Interpenetration of a fabric node

where the corrected contact position, $\boldsymbol{r}_i^{f,corr}(t+\Delta t)$, is given by

$$\boldsymbol{r}_i^{f,corr}(t+\Delta t) = \boldsymbol{r}_i^{f,pred}(t+\Delta t) + \frac{\Delta t^2}{m_i}\boldsymbol{\psi}_i^{con} \tag{4.2}$$

and where the predicted contact position, $\boldsymbol{r}_i^{f,pred}(t+\Delta t)$, is given by[9]

$$\boldsymbol{r}_i^{f,pred}(t+\Delta t) = \boldsymbol{r}_i^{f}(t) + \Delta t(\phi \boldsymbol{v}_i^{f,pred}(t+\Delta t) + (1-\phi)\boldsymbol{v}_i^{f}(t)) \tag{4.3}$$

and

$$\boldsymbol{v}_i^{f,pred}(t+\Delta t) = \boldsymbol{v}_i^{f}(t) + \frac{\Delta t}{m_i}(\phi \boldsymbol{\psi}_i^{f,pred,oth}(t+\Delta t) + (1-\phi)\boldsymbol{\psi}_i^{f,oth}(t)), \tag{4.4}$$

where $\boldsymbol{\psi}_i^{f,oth}$ are all forces *other* than the contact forces. The fabric node is corrected to

$$\boldsymbol{r}_i^{f,pred}(t+\Delta t) = \boldsymbol{r}_i^{p,cp}(t+\Delta t), \tag{4.5}$$

where $\boldsymbol{r}_i^{p,cp}(t+\Delta t)$ is the closest point on the surface of the contacting object (Fig. 3). For an in-depth review of these types of methods see Wriggers [43]. Additionally, we must assign values to the velocity. We first assume that the projectile-fabric surface "sticks". In this case, we assign the velocity of the fabric node to that of the closest point on the body, for node i

$$\boldsymbol{v}_i^{f,corr}(t+\Delta t) = \boldsymbol{v}_i^{p,cp}(t+\Delta t). \tag{4.6}$$

The friction force is that calculated via

$$\boldsymbol{\psi}_i^{fric} = m_i \dot{\boldsymbol{v}}_i - \boldsymbol{\psi}_i^{con} - \boldsymbol{\psi}_i^{f,oth}. \tag{4.7}$$

If the friction force exceeds the theoretical limit

$$||\boldsymbol{\psi}_i^{fric}|| > \mu_s ||\boldsymbol{\psi}_i^{con}||, \tag{4.8}$$

then the assumption that there is "stick" is incorrect, and sliding must occur, resulting in a nonmatching velocity of[10]

$$\boldsymbol{v}_i^{f,corr}(t+\Delta t) = \boldsymbol{v}_i^{f,pred}(t+\Delta t) + \frac{\Delta t}{m_i}(\boldsymbol{\psi}_i^{con} + \boldsymbol{\psi}_i^{fric}), \tag{4.10}$$

with the (frictional) projection

$$\boldsymbol{\psi}_i^{fric} = \mu_d ||\boldsymbol{\psi}_i^{con}|| \frac{\boldsymbol{v}_i^{p,cp} - \boldsymbol{v}_i^{f,cp}}{||\boldsymbol{v}_i^{p,cp} - \boldsymbol{v}_i^{f,cp}||}. \tag{4.11}$$

4.2 Projectile motion

After the calculations culminating with Eq. 4.11 have been completed, the velocity of the projectile is recalculated via (summing the nodal contributions)

$$\boldsymbol{v}^p(t+\Delta t) = \boldsymbol{v}^p(t) - \frac{\Delta t}{m_p}\sum_{i=1}^{N_c}\left(\boldsymbol{\psi}_i^{con} + \boldsymbol{\psi}_i^{fric}\right) + \frac{\Delta t}{m_p}\left(\phi \boldsymbol{\psi}^{p,oth}(t+\Delta t) + (1-\phi)\boldsymbol{\psi}^{p,oth}(t)\right) \tag{4.12}$$

where N_c is the number of nodes in contact, and

$$\boldsymbol{r}^p(t+\Delta t) = \boldsymbol{r}^p(t) + \Delta t(\phi \boldsymbol{v}^p(t+\Delta t) + (1-\phi)\boldsymbol{v}^p(t)). \tag{4.13}$$

The projectile's angular velocity and rotation are determined in a similar manner by integrating the equations for an angular momentum balance

$$\dot{\boldsymbol{H}}_{cm} = \frac{d(\overline{\boldsymbol{I}}\cdot\boldsymbol{\omega})}{dt} = \boldsymbol{M}_{cm}^{EXT}, \tag{4.14}$$

where $\overline{\boldsymbol{I}}$ is the mass moment of the projectile, $\boldsymbol{\omega}$ is the angular velocity and $\boldsymbol{M}_{cm}^{EXT}$ is the sum of all moment contributions external to the projectile, around its center of mass. In Appendix 2, a general rigid body solution algorithm is provided.

5 Model problem: impact of a sphere

As an example, we consider the special case of a spherical projectile, with moment of inertia $I_p^{sphere} = \frac{2}{5}m_p R^2$, where R is the radius of the sphere. In the case of a sphere, the closest point calculation can be determined by calculating a unit vector, denoted $\boldsymbol{n}_{i\to cp}$, from the interpenetrated point and the center of the projectile (Fig. 4)

9 $\boldsymbol{v}_i^f(t)$ is the converged value from the previous time step.

10 We remark that the velocity of any point i on the surface of the body can be determined by simply calculating

$$\boldsymbol{v}_i = \boldsymbol{v}_{cm} + \boldsymbol{\omega}\times\boldsymbol{r}_{cm\to i}. \tag{4.9}$$

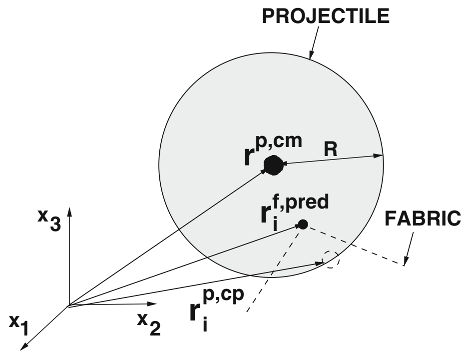

Fig. 4 Closest point projection for a sphere

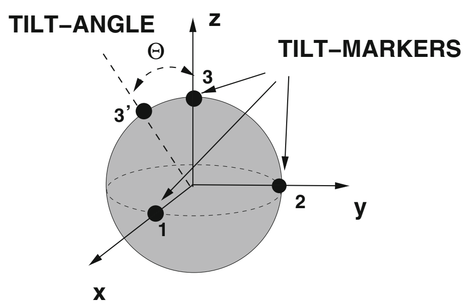

Fig. 5 Markers on a sphere

$$\boldsymbol{r}_i^{f,pred} + \boldsymbol{r}_{i\to cm}^{f,pred} = \boldsymbol{r}_{cm} \Rightarrow \boldsymbol{r}_{i\to cm}^{f,pred} = \boldsymbol{r}_{cm} - \boldsymbol{r}_i^{f,pred}$$
$$\Rightarrow \boldsymbol{n}_{i\to cp} = \frac{\boldsymbol{r}_{cm} - \boldsymbol{r}_i^{f,pred}}{||\boldsymbol{r}_{cm} - \boldsymbol{r}_i^{f,pred}||}, \tag{5.1}$$

and where $\boldsymbol{r}_i^{p,cp} = \boldsymbol{r}_{cm} - R\boldsymbol{n}_{i\to cp}$.

The incoming rigid body was assigned a (center of mass) velocity of 250 m/s and a zero angular velocity. We employ the following measure of inclination, a "tilt-angle" that determines the degree of angular change of "markers" (Fig. 5) placed on the surface of the sphere ($\boldsymbol{r}_m$)

$$\Theta \stackrel{\text{def}}{=} cos^{-1}\left(\frac{(\boldsymbol{r}_m - \boldsymbol{r}^{p,cm}) \cdot (\boldsymbol{r}_{mo} - \boldsymbol{r}^{p,cmo})}{||\boldsymbol{r}_m - \boldsymbol{r}^{p,cm}||||\boldsymbol{r}_{mo} - \boldsymbol{r}^{p,cmo}||}\right). \tag{5.2}$$

The following system parameters were used:[11]

- initial (upper limit) time-step size: $\Delta t = 0.000001$,
- iterative tolerance: TOL = 0.000001,
- sphere radius: $R = 0.02635$ m,
- mass of the projectile: $m_p = 0.037$ kg,
- iteration limit: $K_d = 6$,
- critical stretch ratio for yarn rupture = 1.03,
- yarn radius = 0.000185 m,
- lumped nodes: 100 × 100,
- lumped mass charge $q = 1$,
- external magnetic field $\boldsymbol{B}^{EXT} = 0.05\boldsymbol{e}_x$, (zero electric field, $\boldsymbol{E}^{EXT} = \boldsymbol{0}$),
- the trapezoidal time-stepping parameter $\phi = 0.5$ (midpoint rule),
- static friction coefficient $\mu_s = 1.0$,
- dynamic friction coefficient $\mu_d = 0.95$,
- effective areal density of fabric = 0.12784 kg/m^2 (Zylon (PBO) solid material density = 1540 kg/m^3),
- size of the sheet: 0.254 m × 0.254 m,
- damage rate parameter: $\lambda = 0.1$,
- effective Young's modulus of a yarn $E = 126$ GPa (with statistical variation of 10% from the mean governed by a Gaussian distribution).

The events connected to having no magnetic field can be seen in Figs. 6 and 7 and with a magnetic field in Figs. 8 and 9. The case of no magnetic field produces virtually no spin (Fig. 7). Very slight spin variations occur due to the statistical variation in the Young's modulus from yarn to yarn. Had there been no material variations, the deformation would have been perfectly symmetric, inducing no spin (to within computational machine precision). Clearly, the induced spin is quite large when the $\boldsymbol{v} \times \boldsymbol{B}^{EXT}$ term is present, *due to the breaking of deformation symmetry* (Figs. 8 and 9). This allows the overall friction forces to induce a moment about the projectile's mass center. Notice that the sphere "rocks back and forth" (Fig. 8), which is reflected in Fig. 9 by re-attaining zero tilt value. As in the case of no magnetic field, the normal contact forces produce no moment. The magnetic field induces forces that are proportional to $\boldsymbol{v} \times \boldsymbol{B}^{EXT}$ onto the fabric, which in turn, due to the friction forces, induces reactions onto the contacting object, which can cause it to rotate. This effect is critical in many applications because the tilting of an incoming (non-spherical, ogival) projectile can lead to it being more easily stopped. A rough estimate of how strong of a moment is needed to induce a desired angular "tilt" of Θ^*, can be obtained via a 2-D, "back of the envelope" calculation $I\ddot{\Theta} = M$, where if we consider and object, initially not spinning, undergoing a constant angular acceleration $\Theta(t) = \Theta^* = \Theta_o + \dot{\Theta}(\delta t) + \frac{1}{2}\ddot{\Theta}(\delta t)^2 = \frac{1}{2}\ddot{\Theta}(\delta t)^2$, ($\Theta_o = 0$ and $\dot{\Theta} = 0$) we obtain $\ddot{\Theta} = \frac{2}{(\delta t)^2}\Theta^*$ and, therefore,

$$M = I\frac{2}{(\delta t)^2}\Theta^* = ||\boldsymbol{v}||||\boldsymbol{B}^{EXT}||\mu_s N_c R \tag{5.3}$$

where δt is the time needed (impact interval) for the tilt, Θ^* is the desired amount of tilt, R is the radius of the sphere and N_c is the number of nodes in contact, which is proportional to πR^2, which is a function of the denier of the yarn (the number of yarn per square inch or meter). One can solve for

[11] Corresponding to standard sized projectiles used in our lab at UC Berkeley http://www.me.berkeley.edu/compmat, for nonelectromagnetic materials.

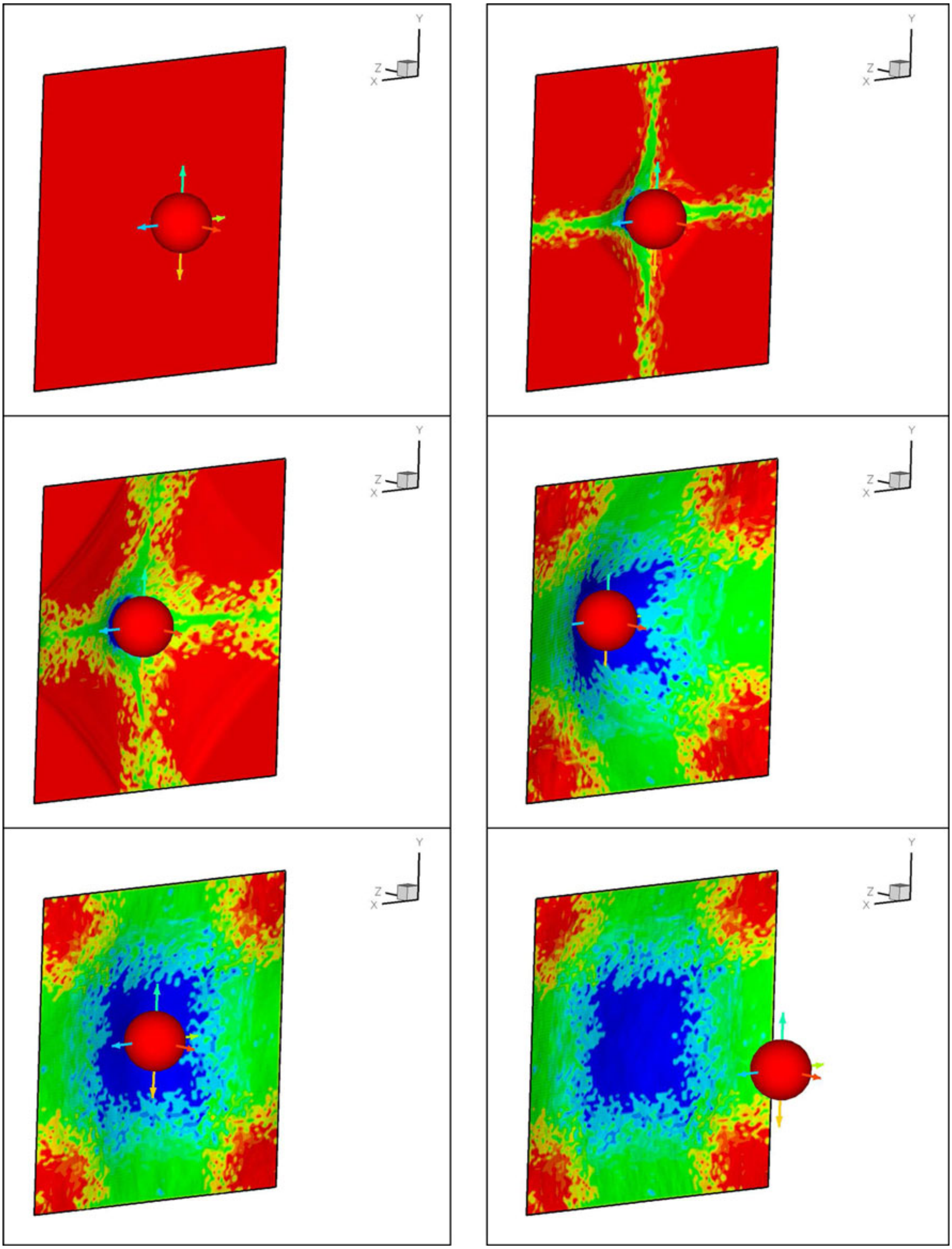

Fig. 6 *Top to bottom* and *left to right*: sequence of impact for an electromagnetically-neutral fabric. *Red* indicates an undamaged material ($\alpha = 1$), while *blue* indicates a highly damaged material ($\alpha = 0$). The *arrows* serve as markers to easily view the projectile orientation

the strength of the magnetic field, yielding

$$||\boldsymbol{B}^{EXT}|| \propto \frac{2I\Theta^*}{(\delta t)^2||\boldsymbol{v}||\mu_s N_c R}, \tag{5.4}$$

which provides a guideline for the magnetic field intensity needed to induced the appropriate moment. This estimate can be sharpened by numerical experiment, such as the one just performed in the model problem.

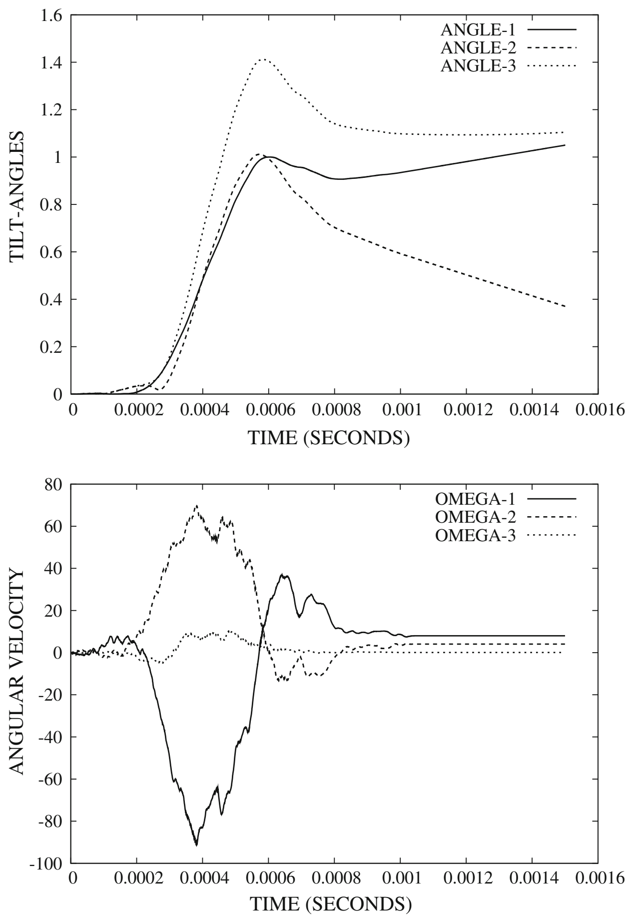

Fig. 7 The induced angular change and spin for an electromagnetically-neutral fabric

6 Summary and extensions

This work developed a formulation for the deformation of fabric structures, addressing (1) the basic mechanics of interconnected yarn networks, (2) simple constitutive relations, including yarn damage, (3) interaction with impacting objects, incorporating contact with friction and (4) electromagnetic sensitivity of the fabric. Of particular interest was the electromagnetic fabric responses, and the illustration of how the Lorentz force, which can cause a torque, can be harnessed to induce spin to an incoming object, whether the impacting object is magnetically sensitive or not. This work addressed scenarios where a rigid object contacted an electromagnetically-sensitive structural fabric and pushed it into an electromagnetic field. The primary interest was the spin induced by the fabric onto the contacting object, which occurs due to the unsymmetric deformation of the fabric.

In many cases, incoming projectiles possess an initial angular velocity. For example, a typical bullet that leaves a rifled muzzle spins along its ogival axis at several thousand radians/sec.[12] Accordingly, consider a rigid object with charged lumped masses attached to its surface. These lumped masses (particles) could be attached to the rigid body through contact with strong friction (Fig. 10). We consider the body to have an angular velocity $\boldsymbol{\omega}$, a center of mass velocity $\boldsymbol{v}_{cm}$, and we assume that the lumped masses are not sliding. As before, the rigid body is not electromagnetically sensitive. The velocity of any point on the body is

$$\boldsymbol{v}_i = \boldsymbol{v}_{cm} + \boldsymbol{\omega} \times \boldsymbol{r}_{cm\to i}. \tag{6.1}$$

If the pushes the lumped masses into a uniform electromagnetic field ($\boldsymbol{E}^{EXT}$, $\boldsymbol{B}^{EXT}$), the external electromagnetic forces acting on each particle are

$$\boldsymbol{\psi}_i^{EXT} = q_i(\boldsymbol{E}^{EXT} + \boldsymbol{v}_i \times \boldsymbol{B}^{EXT}). \tag{6.2}$$

The total external force on the body is

$$\boldsymbol{\Psi}^{EXT} = \sum_{i=1}^{N} \boldsymbol{\psi}_i^{EXT} = q_i(\boldsymbol{E}^{EXT} + \boldsymbol{v}_i \times \boldsymbol{B}^{EXT}), \tag{6.3}$$

and the total external moment about the center of mass of the lumped masses is

$$\begin{aligned}\boldsymbol{M}_{cm}^{EXT} &= \sum_{i=1}^{N} \boldsymbol{r}_{cm\to i} \times \boldsymbol{\psi}_i^{EXT} = \sum_{i=1}^{N} \boldsymbol{r}_{cm\to i} \\ &\quad \times q_i(\boldsymbol{E}^{EXT} + \boldsymbol{v}_i \times \boldsymbol{B}^{EXT}),\end{aligned} \tag{6.4}$$

and the external force can be decomposed into

$$\begin{aligned}\boldsymbol{\Psi}^{EXT} &= \underbrace{\sum_{i=1}^{N} q_i(\boldsymbol{E}^{EXT})}_{\text{electrical contribution}} + \underbrace{\sum_{i=1}^{N} q_i(\boldsymbol{v}_{cm} \times \boldsymbol{B}^{EXT})}_{\text{linear velocity contribution}} \\ &\quad + \underbrace{\sum_{i=1}^{N} q_i((\boldsymbol{\omega} \times \boldsymbol{r}_{cm\to i}) \times \boldsymbol{B}^{EXT})}_{\text{angular velocity contribution}} \\ &= \boldsymbol{E}^{EXT}\left(\sum_{i=1}^{N} q_i\right) + \boldsymbol{v}_{cm} \times \boldsymbol{B}^{EXT}\left(\sum_{i=1}^{N} q_i\right) + \boldsymbol{\omega} \\ &\quad \times \left(\sum_{i=1}^{N} q_i \times \boldsymbol{r}_{cm\to i}\right) \times \boldsymbol{B}^{EXT}\end{aligned} \tag{6.5}$$

[12] This is done to stabilize its flight.

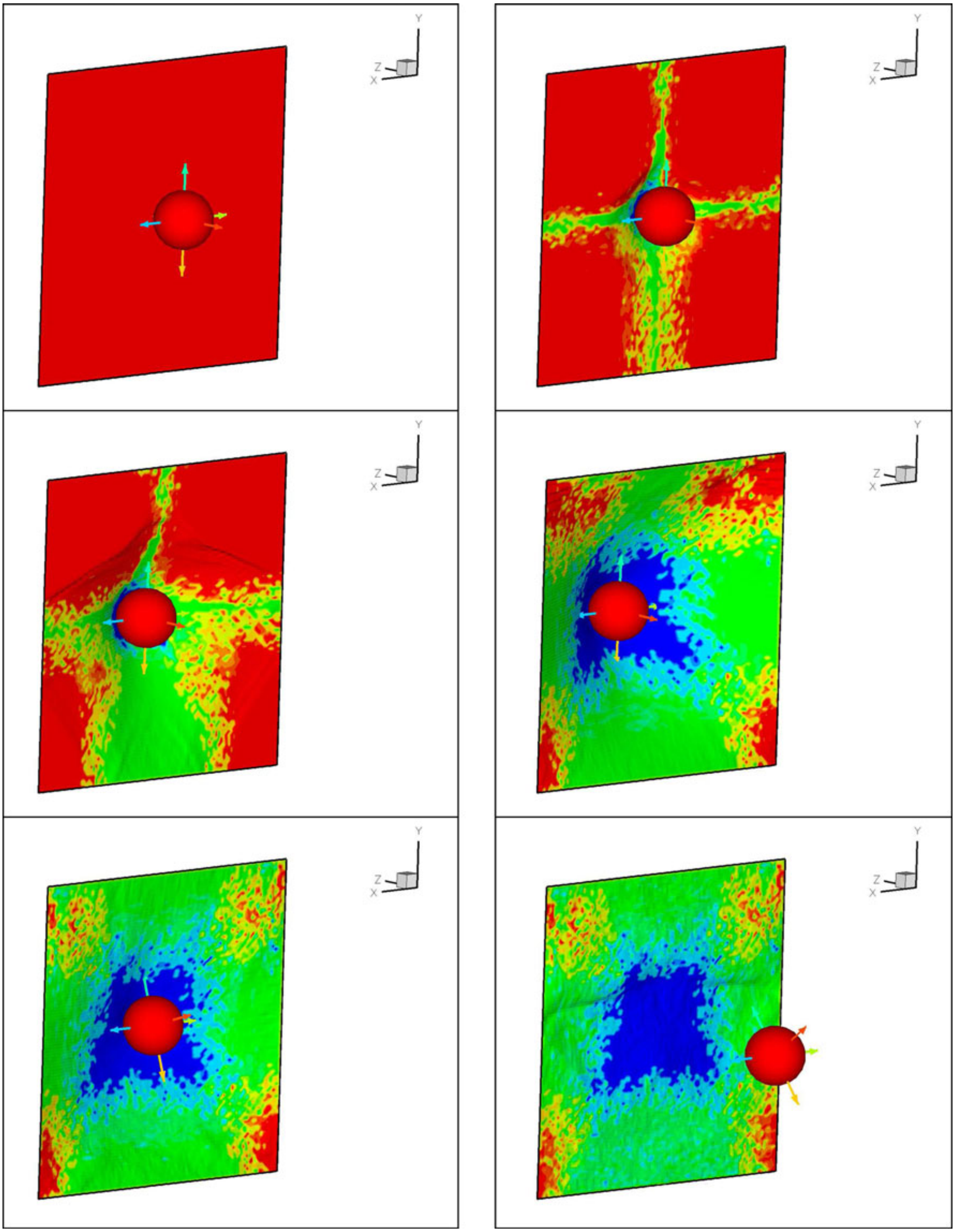

Fig. 8 *Top to bottom* and *left to right*: sequence of impact for an electromagnetically-sensitive fabric. *Red* indicates an undamaged material ($\alpha = 1$), while *blue* indicates a highly damaged material ($\alpha = 0$). The *arrows* serve as markers to easily view the projectile orientation. The important feature to notice is the breaking of symmetry in the deformation, relative the case with no magnetic field

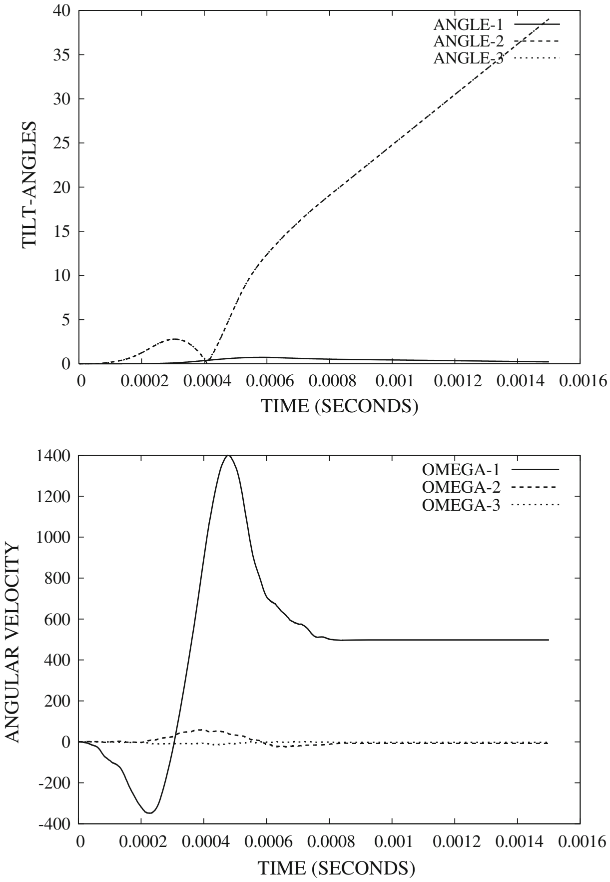

Fig. 9 The induced angular change and spin for an electromagnetically-sensitive fabric. Notice that the sphere "rocks back and forth" (Fig. 8), which is reflected in this plot by passing through a zero tilt value

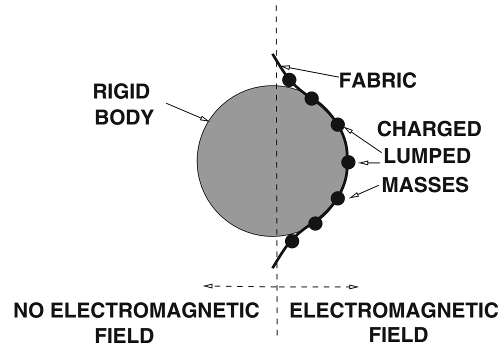

Fig. 10 Lumped masses attached to the surface of a contacting rigid body

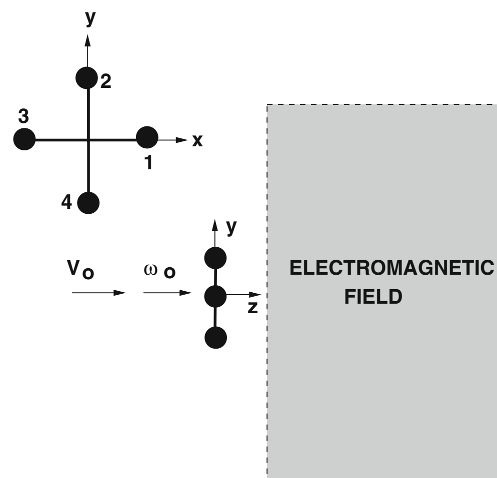

Fig. 11 A set of rigidly fastened charged particles, encountering an electromagnetic field

and the total external moment about the center of mass is

$$
\begin{aligned}
\boldsymbol{M}_{cm}^{EXT} &= \sum_{i=1}^{N} \boldsymbol{r}_{cm\to i} \times \Bigg(\underbrace{q_i(\boldsymbol{E}^{EXT})}_{\text{electrical contribution}} \\
&\quad + \underbrace{q_i(\boldsymbol{v}_{cm} \times \boldsymbol{B}^{EXT})}_{\text{linear velocity contribution}} + \underbrace{q_i((\boldsymbol{\omega} \times \boldsymbol{r}_{cm\to i}) \times \boldsymbol{B}^{EXT})}_{\text{angular velocity contribution}} \Bigg) \\
&= \left(\sum_{i=1}^{N} q_i \boldsymbol{r}_{cm\to i} \right) \times \boldsymbol{E}^{EXT} + \left(\sum_{i=1}^{N} q_i \boldsymbol{r}_{cm\to i} \right) \\
&\quad \times \boldsymbol{v}_{cm} \times \boldsymbol{B}^{EXT} + \left(\sum_{i=1}^{N} q_i \boldsymbol{r}_{cm\to i} \times \boldsymbol{\omega} \times \boldsymbol{r}_{cm\to i} \right) \\
&\quad \times \boldsymbol{B}^{EXT} \\
&= \boldsymbol{r}_q \times \boldsymbol{E}^{EXT} + \boldsymbol{r}_q \times \boldsymbol{v}_{cm} \times \boldsymbol{B}^{EXT} + \boldsymbol{H}_q \times \boldsymbol{B}^{EXT},
\end{aligned}
\tag{6.6}
$$

where we define the following

- $\boldsymbol{r}_q \overset{\text{def}}{=} \sum_{i=1}^{N} q_i \boldsymbol{r}_{cm\to i}$ is the *center of charge with respect to the center of mass* and
- $\boldsymbol{H}_q \overset{\text{def}}{=} \sum_{i=1}^{N} q_i \frac{\boldsymbol{H}_{i/o}}{m_i}$ is the *charged angular momentum per unit mass with respect to the center of mass.*

These observations provide a "snapshot" of the electromagnetic forces and moments that would produced by the charged masses.

To illustrate the forces that induce the rotation, now let us consider the specific case of an object comprised of four charged particles rigidly fastened together (Fig. 11).[13] Also consider the initial spin of the object about its longitudinal axis, $\boldsymbol{\omega} = \omega_o \boldsymbol{k}$, and center of mass velocity of $\boldsymbol{v}_{cm} = v_o \boldsymbol{k}$ as depicted in Fig. 11. The locations of the particles are

$$
\boldsymbol{r}_1 = R\boldsymbol{i},\ \ \boldsymbol{r}_2 = R\boldsymbol{j},\ \ \boldsymbol{r}_3 = -R\boldsymbol{i} \text{ and } \boldsymbol{r}_4 = -R\boldsymbol{j}, \tag{6.7}
$$

[13] It may help the reader to imagine that they are fastened together with rigid, massless, rods.

with corresponding total velocities given by

$$\boldsymbol{v}_i = v_o \boldsymbol{k} + \omega_o \boldsymbol{k} \times \boldsymbol{r}_{cm\to i}. \tag{6.8}$$

Let us "itemize" the contributions to the forces and moments from this initial encounter:

- Induced force due to the electric field:

$$\boldsymbol{\Psi}^{EXT,E} = \sum_{i=1}^{N_c} \boldsymbol{\psi}_i^{EXT,E} = \left(\boldsymbol{E}_x^{EXT}\boldsymbol{i} + \boldsymbol{E}_y^{EXT}\boldsymbol{j} + \boldsymbol{E}_z^{EXT}\boldsymbol{k}\right)\left(\sum_{i=1}^{N_c} q_i\right) \tag{6.9}$$

- Induced force due to the linear motion and the magnetic field:

$$\begin{aligned}\boldsymbol{\psi}_i^{EXT,B,lin} &= \sum_{i=1}^{N_c} \boldsymbol{\psi}_i^{EXT,B,lin} \\ &= \left(-\boldsymbol{B}_y^{EXT} v_o \boldsymbol{i} + \boldsymbol{B}_x^{EXT} v_o \boldsymbol{j}\right)\left(\sum_{i=1}^{N_c} q_i\right)\end{aligned} \tag{6.10}$$

- Induced force due to the rotational motion and the magnetic field:

$$\begin{aligned}\boldsymbol{\Psi}^{EXT,B,rot} &= \sum_{i=1}^{N_c} \boldsymbol{\psi}_i^{EXT,B,rot} \\ &= (q_1 - q_3)\left(\boldsymbol{B}_z^{EXT}\omega_o R\boldsymbol{i} - \boldsymbol{B}_x^{EXT}\omega_o R\boldsymbol{k}\right) \\ &\quad + (q_2 - q_4)\left(\boldsymbol{B}_z^{EXT}\omega_o R\boldsymbol{j} - \boldsymbol{B}_y^{EXT}\omega_o R\boldsymbol{k}\right)\end{aligned} \tag{6.11}$$

- Induced moment due to the electric field:

$$\begin{aligned}\boldsymbol{M}^{EXT,E} &= \sum_{i=1}^{N_c} \boldsymbol{M}_i^{EXT,E} \\ &= R\boldsymbol{E}_z^{EXT}\left((q_2 - q_4)\boldsymbol{i} + (q_3 - q_1)\boldsymbol{j}\right) \\ &\quad + R\left(\boldsymbol{E}_y^{EXT}(q_1 - q_3) + \boldsymbol{E}_x^{EXT}(q_4 - q_2)\right)\boldsymbol{k}.\end{aligned} \tag{6.12}$$

- Induced moment due to linear motion and the magnetic field:

$$\begin{aligned}\boldsymbol{M}^{EXT,B,lin} &= \sum_{i=1}^{N_c} \boldsymbol{M}_i^{EXT,B,lin} \\ &= v_o R\left((q_3 - q_1)\boldsymbol{B}_y^{EXT}\boldsymbol{i} + (q_2 - q_4)\boldsymbol{B}_x^{EXT}\boldsymbol{j}\right)\end{aligned} \tag{6.13}$$

- Induced moment due to rotational motion and the magnetic field:

$$\begin{aligned}\boldsymbol{M}^{EXT,E,rot} &= \sum_{i=1}^{N_c} \boldsymbol{M}_i^{EXT,B,rot} \\ &= \omega_o R^2\left(-(q_2 + q_4)\boldsymbol{B}_y^{EXT}\boldsymbol{i}\right. \\ &\quad \left. + (q_1 + q_3)\boldsymbol{B}_x^{EXT}\boldsymbol{j}\right)\end{aligned} \tag{6.14}$$

We have the following observations:

1. If $\sum_{i=1}^{4} q_i = 0$, then the magnetic contribution due to the linear velocity is zero.
2. If $\sum_{i=1}^{4} q_i = 0$, then the electric contribution is zero.
3. If $q_1 = q_3$ and $q_4 = q_2$, then the electric field contributes no moment.
4. If $q_1 = q_3$ and $q_4 = q_2$, then the magnetic contribution due to the linear velocity is zero.
5. If $q_2 = -q_4$ and $q_1 = -q_3$, then the magnetic contribution due to the angular velocity is zero.
6. Most importantly, Eq. 6.14 asserts that, if $q_2 = q_4$ and $q_1 = q_3$, then the magnetic contribution due to the rotational velocity will tend to rotate the body, provided that B_y^{EXT} and/or B_x^{EXT} are nonzero.

These observations only hold for the initial force and moments generated when the object just encounters the electromagnetic field. Thereafter, the dynamics must be treated numerically, for example using the techniques discussed in this paper. Accordingly, Fig. 12 illustrates the results for $\omega_{0z} = 10000$ rad/s. Notice the increase in the angular velocity in the y-direction, which reached a final value of approximately 147 rad/s, as opposed to nearly zero (Fig. 9) for the case when the initial angular velocity was $\omega_{0z} = 0$. Further numerical investigation of this effect, as well as experiments are currently under way at the author's laboratory at UC Berkeley http://www.me.berkeley.edu/compmat. As we have mentioned earlier in the paper, the sensitivity of the fabric to electromagnetic fields can be induced by seeding small-scale (nano) particles within the weave. Such approaches are currently being explored by the author to produce durable electromagnetically sensitive fabric.

Finally, a variety of extensions to the model are possible, in particular, involving the sensing and actuation of electromagnetically sensitive networks of biological materials. For example, instead of a Kirchhoff St. Venant type model used earlier, one can consider a one-dimensional Fung material model for the yarn (Fung [12]).[14] The stored energy of a

[14] The well-known difficulties and ambiguities with the three-dimensional Fung model are irrelevant for this one-dimensional analysis. Fibrous material represents the load bearing component of many types

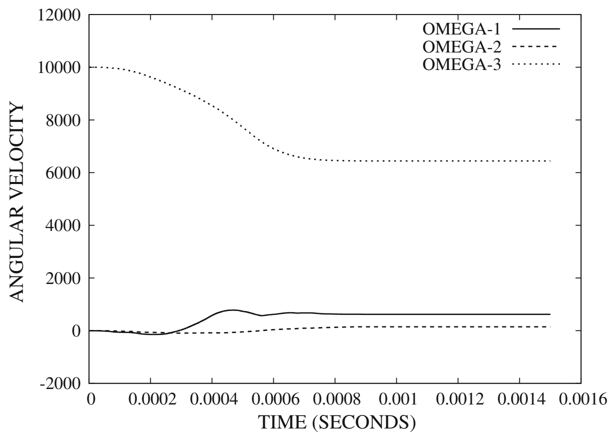

Fig. 12 The induced angular change and spin for an electromagnetically-sensitive fabric with initial angular velocity of $\omega_{0z} = 10000$ rad/s. Notice the increase in the angular velocity in the y-direction, which reached a final value of approximately 147 rad/s, as opposed to nearly zero for the case when the initial angular velocity was $\omega_{0z} = 0$

single Fung fiber is given by $W = c(e^Q - 1)$, where $Q = \frac{1}{2}HE^2$, H and c are material constants, $E \stackrel{\text{def}}{=} \frac{1}{2}(U^2 - 1)$ is the Green-Lagrange strain. The exponential term phenomenologically describes a stiffening effect, due to a progressive reduction in fibrous microscale "slack", which is prevalent in many types biological tissue. The second Piola–Kirchhoff stress is given by $S = \frac{\partial W}{\partial E} = c\frac{\partial Q}{\partial E}e^Q = cHEe^{\frac{HE^2}{2}}$. Thereafter, the approach is identical to what has been presented in the body of this work. Experiments on electromagnetically induced actuation of biological tissue, and the actual construction of such materials, is also an area of current study by the author.

Appendix 1: time-stepping

In order motivate the time-stepping scheme, we first start with the dynamics of a single lumped mass. The equation of motion is given by

$$m_i \dot{\boldsymbol{v}}_i = \boldsymbol{\psi}_i^{tot}, \tag{A1}$$

where $\boldsymbol{\psi}_i^{tot}$ is the total force provided from interactions with the external environment (yarn, contact, electromagnetics, etc). Expanding the velocity in a Taylor series about $t + \phi\Delta t$ we obtain

$$\boldsymbol{v}_i(t+\Delta t) = \boldsymbol{v}_i(t+\phi\Delta t) + \frac{d\boldsymbol{v}_i}{dt}|_{t+\phi\Delta t}(1-\phi)\Delta t + \frac{1}{2}\frac{d^2\boldsymbol{v}_i}{dt^2}|_{t+\phi\Delta t}(1-\phi)^2(\Delta t)^2 + \mathcal{O}(\Delta t)^3 \tag{A2}$$

and

$$\boldsymbol{v}_i(t) = \boldsymbol{v}_i(t+\phi\Delta t) - \frac{d\boldsymbol{v}_i}{dt}|_{t+\phi\Delta t}\phi\Delta t + \frac{1}{2}\frac{d^2\boldsymbol{v}_i}{dt^2}|_{t+\phi\Delta t}\phi^2(\Delta t)^2 + \mathcal{O}(\Delta t)^3 \tag{A3}$$

Subtracting the two expressions yields

$$\frac{d\boldsymbol{v}_i}{dt}|_{t+\phi\Delta t} = \frac{\boldsymbol{v}_i(t+\Delta t) - \boldsymbol{v}_i(t)}{\Delta t} + \hat{\mathcal{O}}(\Delta t), \tag{A4}$$

where $\hat{\mathcal{O}}(\Delta t) = \mathcal{O}(\Delta t)^2$, when $\phi = \frac{1}{2}$. Thus, inserting this into the equations of equilibrium yields

$$\boldsymbol{v}_i(t+\Delta t) = \boldsymbol{v}_i(t) + \frac{\Delta t}{m_i}\boldsymbol{\psi}_i^{tot}(t+\phi\Delta t) + \hat{\mathcal{O}}(\Delta t)^2. \tag{A5}$$

Note that adding a weighted sum of Eqs. A2 and A3 yields

$$\boldsymbol{v}_i(t+\phi\Delta t) = \phi\boldsymbol{v}_i(t+\Delta t) + (1-\phi)\boldsymbol{v}_i(t) + \mathcal{O}(\Delta t)^2, \tag{A6}$$

which will be useful shortly. Now expanding the position of the center of mass in a Taylor series about $t + \phi\Delta t$ we obtain

$$\boldsymbol{r}_i(t+\Delta t) = \boldsymbol{r}_i(t+\phi\Delta t) + \frac{d\boldsymbol{r}_i}{dt}|_{t+\phi\Delta t}(1-\phi)\Delta t + \frac{1}{2}\frac{d^2\boldsymbol{r}_i}{dt^2}|_{t+\phi\Delta t}(1-\phi)^2(\Delta t)^2 + \mathcal{O}(\Delta t)^3 \tag{A7}$$

and

$$\boldsymbol{r}_i(t) = \boldsymbol{r}_i(t+\phi\Delta t) - \frac{d\boldsymbol{r}_i}{dt}|_{t+\phi\Delta t}\phi\Delta t + \frac{1}{2}\frac{d^2\boldsymbol{r}_i}{dt^2}|_{t+\phi\Delta t}\phi^2(\Delta t)^2 + \mathcal{O}(\Delta t)^3. \tag{A8}$$

Subtracting the two expressions yields

$$\frac{\boldsymbol{r}_i(t+\Delta t) - \boldsymbol{r}_i(t)}{\Delta t} = \boldsymbol{v}_i(t+\phi\Delta t) + \hat{\mathcal{O}}(\Delta t). \tag{A9}$$

Inserting Eq. A6 yields

$$\boldsymbol{r}_i(t+\Delta t) = \boldsymbol{r}_i(t) + (\phi\boldsymbol{v}_i(t+\Delta t) + (1-\phi)\boldsymbol{v}_i(t))\,\Delta t + \hat{\mathcal{O}}(\Delta t)^2. \tag{A10}$$

and thus using Eq. A5 yields

$$\boldsymbol{r}_i(t+\Delta t) = \boldsymbol{r}_i(t) + \boldsymbol{v}_i(t)\Delta t + \frac{\phi(\Delta t)^2}{m_i}\boldsymbol{\psi}_i^{tot}(t+\phi\Delta t) + \hat{\mathcal{O}}(\Delta t)^2. \tag{A11}$$

The term $\boldsymbol{\psi}_i^{tot}(t+\phi\Delta t)$ can be approximated by $\boldsymbol{\psi}_i^{tot}(t+\phi\Delta t) \approx \phi\boldsymbol{\psi}_i^{tot}(\boldsymbol{r}_i(t+\Delta t)) + (1-\phi)\boldsymbol{\psi}_i^{tot}(\boldsymbol{r}_i(t))$. Thus, we

Footnote14 continued
of soft biological tissue. For overviews of a wide variety of soft tissue continuum models, see the review found in Humphrey [17]. Models which explicitly account for the presence of fibers in biological tissue date back, at least, to Lanir [21], who formulated continuum models based on the existence of fiber families. For a review of Lanir-type models, as well as other classes of biological constitutive models, see the review of Sacks and Sun [32]. Also see the work of Costa et al. [8] and Zohdi [51], among numerous others.

have the following for the velocity[15]

$$\boldsymbol{v}_i(t+\Delta t)=\boldsymbol{v}_i(t)+\frac{\Delta t}{m_i}\left(\phi\boldsymbol{\psi}_i^{tot}(t+\Delta t)\right.\\ \left.+(1-\phi)\boldsymbol{\psi}_i^{tot}(t)\right) \tag{A12}$$

and for the position

$$\boldsymbol{r}_i(t+\Delta t)=\boldsymbol{r}_i(t)+\boldsymbol{v}_i(t+\phi\Delta t)\Delta t\\ =\boldsymbol{r}_i(t)+(\phi\boldsymbol{v}_i(t+\Delta t)+(1-\phi)\boldsymbol{v}_i(t))\,\Delta t, \tag{A13}$$

or, explicitly combining the expressions,

$$\boldsymbol{r}_i(t+\Delta t)=\boldsymbol{r}_i(t)+\boldsymbol{v}_i(t)\Delta t+\frac{\phi(\Delta t)^2}{m_i}\left(\phi\boldsymbol{\psi}_i^{tot}(t+\Delta t)\right.\\ \left.+(1-\phi)\boldsymbol{\psi}_i^{tot}(t)\right). \tag{A14}$$

Appendix 2: numerical methods for the dynamics of a rigid body

Since the translational motion of the rigid body has been already considered in the main part of the paper, we now turn to the rotational contribution. There are two, more or less, equivalent approaches to compute the rotations using a (1) Inertially-fixed frame and (2) Body-fixed frame. We employ an inertially-fixed approach for the duration of the presentation.[16] This approach entails, at each (implicit) time step, decomposing an increment of motion into an incremental rigid body translational contribution and an incremental rigid body rotational contribution (rotation about the center of mass). The rotational contribution is determined by solving a set of coupled nonlinear equations governing the angular velocity and the incremental rotation of the body around the axis of rotation (which also changes as a function of time, and must also be determined). The equation for the angular momentum can be written using fixed inertial coordinates

$$\dot{\boldsymbol{H}}_{cm}=\frac{d(\overline{\boldsymbol{I}}\cdot\boldsymbol{\omega})}{dt}=\boldsymbol{M}_{cm}^{EXT}. \tag{B1}$$

Because the body rotates, the moment of inertia about the center of mass, $\overline{\boldsymbol{I}}$, is implicitly dependent on $\boldsymbol{\omega}$ (and hence time), which leads to a coupled system of nonlinear ODE's, which will be solved with an iterative scheme. Equation B1 is discretized by a trapezoidal scheme

$$\frac{d(\overline{\boldsymbol{I}}\cdot\boldsymbol{\omega})}{dt}|_{t+\phi\Delta t}=\frac{(\overline{\boldsymbol{I}}\cdot\boldsymbol{\omega})|_{t+\Delta t}-(\overline{\boldsymbol{I}}\cdot\boldsymbol{\omega})|_t}{\Delta t}. \tag{B2}$$

thus leading to

$$(\overline{\boldsymbol{I}}\cdot\boldsymbol{\omega})|_{t+\Delta t}=(\overline{\boldsymbol{I}}\cdot\boldsymbol{\omega})|_t+\Delta t\boldsymbol{M}_{cm}^{EXT}(t+\phi\Delta t). \tag{B3}$$

Solving for $\boldsymbol{\omega}(t+\Delta t)$ yields

$$\boldsymbol{\omega}(t+\Delta t)=\left(\overline{\boldsymbol{I}}(t+\Delta t)\right)^{-1}\\ \cdot\left((\overline{\boldsymbol{I}}\cdot\boldsymbol{\omega})|_t+\Delta t\boldsymbol{M}_{cm}^{EXT}(t+\phi\Delta t)\right), \tag{B4}$$

where

$$\boldsymbol{M}_{cm}^{EXT}(t+\phi\Delta t)\approx\phi\boldsymbol{M}_{cm}^{EXT}(t+\Delta t)\\ +(1-\phi)\boldsymbol{M}_{cm}^{EXT}(t) \tag{B5}$$

which yields an implicit nonlinear equation, of the form $\boldsymbol{\omega}(t+\Delta t)=\mathcal{F}(\boldsymbol{\omega}(t+\Delta t))$, since $\overline{\boldsymbol{I}}(t+\Delta t)$, due to the body's rotation. An iterative, implicit, solution scheme may be written as follows for $K=1,2\ldots$

$$\boldsymbol{\omega}^{K+1}(t+\Delta t)=\left(\overline{\boldsymbol{I}}^K(t+\Delta t)\right)^{-1}\\ \cdot\left((\overline{\boldsymbol{I}}\cdot\boldsymbol{\omega})|_t+\Delta t\boldsymbol{M}_{cm}^{EXT,K}(t+\phi\Delta t)\right), \tag{B6}$$

where $\overline{\boldsymbol{I}}^K(t+\Delta t)$ can be computed by a similarity transform (described shortly).[17] After the update for $\boldsymbol{\omega}^{K+1}(t+\Delta t)$ has been computed (utilizing the $\overline{\boldsymbol{I}}^K(t+\Delta t)$ from the previous iteration), the rotation of the body about the center of mass can be determined. The *incremental* angular rotation around the instantaneous rotation axis $\boldsymbol{a}^{K+1}(t+\phi\Delta t)$ (which will also have to be updated) is obtained by

$$\frac{d\theta^{K+1}}{dt}(t+\phi\Delta t)=\omega^{K+1}(t+\phi\Delta t)\\ \approx\frac{\Delta\theta^{K+1}(t+\phi\Delta t)}{\Delta t} \tag{B7}$$

where $\boldsymbol{\omega}^{K+1}(t+\phi\Delta t)=\omega^{K+1}(t+\phi\Delta t)\boldsymbol{a}^{K+1}(t+\phi\Delta t)$, $\omega^{K+1}(t+\phi\Delta t)$ being *a scalar* rotation about the instantaneous axis,

$$\boldsymbol{a}^{K+1}(t+\phi\Delta t)\overset{\text{def}}{=}\frac{\boldsymbol{\omega}^{K+1}(t+\phi\Delta t)}{||\boldsymbol{\omega}^{K+1}(t+\phi\Delta t)||}\\ \approx\frac{\phi\boldsymbol{\omega}^{K+1}(t+\Delta t)+(1-\phi)\boldsymbol{\omega}(t)}{||\phi\boldsymbol{\omega}^{K+1}(t+\Delta t)+(1-\phi)\boldsymbol{\omega}(t)||}, \tag{B8}$$

and thus

$$\Delta\theta^{K+1}(t+\phi\Delta t)=\omega^{K+1}(t+\phi\Delta t)\Delta t, \tag{B9}$$

where $\omega^{K+1}(t+\Delta t)=||\phi\boldsymbol{\omega}^{K+1}(t+\Delta t)+(1-\phi)\boldsymbol{\omega}(t)||$. To determine the movement of the individual points on the rigid body, we need to perform a rigid body translation and rotation (described in the next section). For example, consider a

[15] In order to streamline the notation, we drop the cumbersome $\mathcal{O}(\Delta t)$-type terms.

[16] For a body-fixed formulation, see Powell and Zohdi [29].

[17] One may view the overall process as a fixed-point calculation of the form $\boldsymbol{\omega}^{K+1}(t+\Delta t)=\mathcal{F}(\boldsymbol{\omega}^K(t+\Delta t))$.

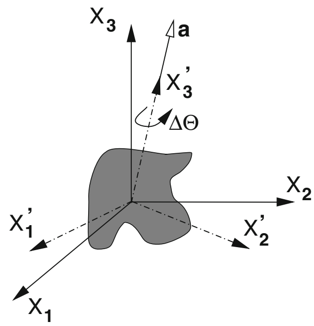

Fig. 13 Aligning the primed coordinate system with the instantaneous axis of rotation (for a general body)

point $\boldsymbol{r}_i$ on the body. The update would be

$$\boldsymbol{r}_i(t+\Delta t) = \boldsymbol{r}_i(t) + \underbrace{\boldsymbol{u}_{cm}}_{due\ to\ cm\ translation} + \underbrace{\boldsymbol{u}_{i,rot}}_{due\ to\ rotation\ wrt\ cm} \tag{B10}$$

where $\boldsymbol{u}_{cm} = \boldsymbol{r}_{cm}(t+\Delta t) - \boldsymbol{r}_{cm}(t)$ and where $\boldsymbol{u}_{i,rot}$ is contribution due to an incremental rotation of the relative position vector

$$\boldsymbol{\tau}^{(i)} \stackrel{\mathrm{def}}{=} \boldsymbol{r}_i(t) - \boldsymbol{r}_{cm}(t) \tag{B11}$$

by $\Delta\theta$ about the cm (Fig. 13).

Transformation matrices for updates and incremental rotation

In order to rotate any point i associated with the rigid body, with position vector $\boldsymbol{\tau}^{(i)}$ we require some standard transformations. The same transformation are needed to rotate the body's moment of inertia, $\overline{\boldsymbol{I}}$. It is a relatively standard exercise in linear algebra to show that any vector, $\boldsymbol{\tau}$, which can be expressed in either the unprimed or primed basis, $\boldsymbol{\tau} = (\boldsymbol{\tau}\cdot\boldsymbol{e}_i)\boldsymbol{e}_i = (\boldsymbol{\tau}\cdot\boldsymbol{e}'_j)\boldsymbol{e}'_j$ where summation index notation is employed. These two representations are explicitly related by

$$\begin{bmatrix}\tau_1\\ \tau_2\\ \tau_3\end{bmatrix}' = \underbrace{\begin{bmatrix}\boldsymbol{e}_1\cdot\boldsymbol{e}'_1 & \boldsymbol{e}_2\cdot\boldsymbol{e}'_1 & \boldsymbol{e}_3\cdot\boldsymbol{e}'_1\\ \boldsymbol{e}_1\cdot\boldsymbol{e}'_2 & \boldsymbol{e}_2\cdot\boldsymbol{e}'_2 & \boldsymbol{e}_3\cdot\boldsymbol{e}'_2\\ \boldsymbol{e}_1\cdot\boldsymbol{e}'_3 & \boldsymbol{e}_2\cdot\boldsymbol{e}'_3 & \boldsymbol{e}_3\cdot\boldsymbol{e}'_3\end{bmatrix}}_{[\boldsymbol{A}]}\begin{bmatrix}\tau_1\\ \tau_2\\ \tau_3\end{bmatrix}. \tag{B12}$$

Note that $\boldsymbol{A}^{-1} = \boldsymbol{A}^T$, thus $\boldsymbol{\tau}' = \boldsymbol{A}\cdot\boldsymbol{\tau}$ and $\boldsymbol{\tau} = \boldsymbol{A}^T\cdot\boldsymbol{\tau}'$. This basic result can be used to perform rotation of a vector about an axis, as well as the rotation of the inertia tensor. Without any loss of generality, we align the $\boldsymbol{e}'_3$ axis to instantaneous rotation axis $\boldsymbol{a}$. The total transformation (rotation) of a vector $\boldsymbol{\tau}^{(i)}$ representing a point i on the body, can be represented by

$$[\boldsymbol{\tau}^{(i)}]^{rot} = \underbrace{[\boldsymbol{A}]^T\,\underbrace{[\boldsymbol{R}(\Delta\theta)]\,\underbrace{[\boldsymbol{A}][\boldsymbol{\tau}_i]}_{[\boldsymbol{\tau}^{(i)}]'}}_{[\boldsymbol{\tau}^{(i)}]^{rot,\prime}}}_{[\boldsymbol{\tau}^{(i)}]^{rot}} \tag{B13}$$

where

$$[\boldsymbol{R}(\Delta\theta)] = \begin{bmatrix}\cos(\Delta\theta) & -\sin(\Delta\theta) & 0\\ \sin(\Delta\theta) & \cos(\Delta\theta) & 0\\ 0 & 0 & 1\end{bmatrix} \tag{B14}$$

Similarly, for the rotation inertia tensor

$$[\overline{\boldsymbol{I}}]^{rot} = \underbrace{[\boldsymbol{A}]\,\underbrace{[\boldsymbol{R}(\Delta\theta)]^T\,\underbrace{[\boldsymbol{A}]^T[\overline{\boldsymbol{I}}][\boldsymbol{A}]}_{[\overline{\boldsymbol{I}}]'}[\boldsymbol{R}(\Delta\theta)]}_{[\overline{\boldsymbol{I}}]^{rot,\prime}}[\boldsymbol{A}]^T}_{[\overline{\boldsymbol{I}}]^{rot}}, \tag{B15}$$

where, during the iterative calculations, $[\overline{\boldsymbol{I}}] = [\overline{\boldsymbol{I}}(t)]$ and $[\overline{\boldsymbol{I}}]^{rot} = [\overline{\boldsymbol{I}}(t+\Delta t))]$.

Algorithmic procedure

The overall procedure is as follows, at time t:

1. Compute the new position of the center of mass.
2. Compute (iteratively) the incremental angular rotation of the body with respect to the center of mass until system convergence:

$$||\boldsymbol{\omega}^{K+1}(t+\Delta t) - \boldsymbol{\omega}^K(t+\Delta t)|| \le TOL||\boldsymbol{\omega}^{K+1}(t+\Delta t)||. \tag{B16}$$

This requires a rotation of the body within the iterations:

(a) Given that $\boldsymbol{\omega}^{K+1}(t+\Delta t)$ has been computed

$$\boldsymbol{\omega}^{K+1}(t+\Delta t) = \left(\overline{\boldsymbol{I}}^K(t+\Delta t)\right)^{-1} \cdot\left((\overline{\boldsymbol{I}}\cdot\boldsymbol{\omega})|_t + \Delta t\boldsymbol{M}_{cm}^{EXT,K}(t+\phi\Delta t)\right) \tag{B17}$$

(b) Compute the (updated) axis of rotation:

$$\boldsymbol{a}^{K+1}(t+\phi\Delta t) \stackrel{\mathrm{def}}{=} \frac{\boldsymbol{\omega}^{K+1}(t+\phi\Delta t)}{||\boldsymbol{\omega}^{K+1}(t+\phi\Delta t)||} \approx \frac{\phi\boldsymbol{\omega}^{K+1}(t+\Delta t) + (1-\phi)\boldsymbol{\omega}(t)}{||\phi\boldsymbol{\omega}^{K+1}(t+\Delta t) + (1-\phi)\boldsymbol{\omega}(t)||}. \tag{B18}$$

(c) Compute the basis $\boldsymbol{e}'_3$-aligned instantaneous axis of rotation:
   (i) $\boldsymbol{e}'_3$, is aligned with $\boldsymbol{a}^{K+1}(t+\Delta t)$

(ii) $e_1' = e_3' \times e_3 / ||e_3' \times e_3||$ and
(iii) $e_2' = e_3' \times e_1' / ||e_3' \times e_1'||$

(d) Compute the composite transformation for the inertia tensor in Eq. B15 and obtain the update $\overline{I}^{K+1}(t + \Delta t)$.

(e) Repeat steps (a)–(d) until Eq. B17 is satisfied.

3. Compute the total new position of the points on the body (i) with Eq. B13, increment time forward and repeat the procedure.

References

1. Atai AA, Steigmann DJ (1997) On the nonlinear mechanics of discrete networks. Arch Appl Mech 67:303–319
2. Atai AA, Steigmann DJ (1998) Coupled deformations of elastic curves and surfaces. Int J Solids Struct 35(16):1915–1952
3. Buchholdt HA, Davies M, Hussey MJL (1968) The analysis of cable nets. J Inst Maths Appl 4:339–358
4. Bufler H, Nguyen-Tuong B (1980) On the work theorems in nonlinear network theory. Ing Arch 49:275–286
5. Cannarozzi M (1987) A minimum principle for tractions in the elastostatics of cable networks. Int J Solids Struct 23:551–568
6. Cannarozzi M (1985) Stationary and extremum variational formulations for the elastostatics of cable networks. Meccanica 20:136–143
7. Cheeseman BA, Bogetti TA (2003) Ballistic impact into fabric and compliant composite laminates. Compos Struct 61:161–173
8. Costa KD, Holmes JW, McCulloch AD (2001) Modeling cardiac mechanical properties in three dimensions. Phil Trans R Soc Lond A 359:1233–1250
9. Duan Y, Keefe M, Bogetti TA, Cheeseman BA (2005) Modeling the role of friction during ballistic impact of a high-strength plain-weave fabric. Compos Struct 68:331–337
10. Duan Y, Keefe M, Bogetti TA, Cheeseman BA (2005) Modeling friction effects on the ballistic impact behavior of a single-ply high strength fabric. Int J Impact Eng 31:996–1012
11. Duan Y, Keefe M, Bogetti TA, Powers B (2006) Finite element modeling of transverse impact on a ballistic fabric. Int J Mech Sci 48:33–43
12. Fung YC (1983) On the foundations of biomechanics. ASME J Appl Mech 50:1003–1009
13. Godfrey TA, Rossettos JN (1999) The onset of tear propagation at slits in stressed uncoated plain weave fabrics. J Appl Mech 66:926–933
14. Haseganu EM, Steigmann DJ (1994) Analysis of partly wrinkled membranes by the method of dynamic relaxation. Comput Mech 14:596–614
15. Haseganu EM, Steigmann DJ (1994) Theoretical flexural response of a pressurized cylindrical membrane. Int J Solids Struct 31:27–50
16. Haseganu EM, Steigmann DJ (1996) Equilibrium analysis of finitely deformed elastic networks. Comput Mech 17:359–373
17. Humphrey JD (2002) Cardiovascular solid mechanics. Cells, tissues, and organs. Springer-Verlag, New York
18. Johnson GR, Beissel SR, Cunniff PM (1999) A computational model for fabrics subjected to ballistic impact. In: Proceedings of the 18th international symposium on ballistics, San Antonio, TX, pp 962–969
19. Kollegal MG, Sridharan S (2000) Strength prediction of plain woven fabrics. J Compos Mater 34:240–257
20. Kwong K, Goldsmith W (2004) Lightweight ballistic protection of flight-critical components on commercial aircraft—ballistic characterization of Zylon. FAA report DOT/FAA/AR-04/45, P1
21. Lanir Y (1983) Constitutive equations for fibrous connective tissues. J Biomech 16(1):1–12
22. Lim CT, Tan VBC, Cheong CH (2002) Perforation of high-strength double-ply fabric system by varying shaped projectiles. Int J Impact Eng 27:577–591
23. Lim CT, Shim VPW, Ng YH (2003) Finite-element modeling of the ballistic impact of fabric armor. Int J Impact Eng 28:13–31
24. Meyers MA (1994) Dynamic behavior of materials. Wiley, New York
25. Pangiotopoulos PD (1976) A variational inequality approach to the inelastic stress-unilateral analysis of cable structures. Comput Struct 6:133–139
26. Papadrakakis M (1980) A method for the automatic evaluation of the dynamic relaxation parameters. Comput Methods Appl Mech Eng 25:35–48
27. Pipkin AC (1986) The relaxed energy density for isotropic elastic membranes. IMA J Appl Math 36:297–308
28. Powell D, Zohdi T, Johnson G (2008) Multiscale modeling of structural fabric undergoing impact. FAA report DOT/FAA/AR-08/38
29. Powell D, Zohdi T (2009) Attachment mode performance of network-modeled ballistic fabric shielding. Composites B 40(6):451–460
30. Rossettos JN, Godfrey TA (2003) Effect of slipping yarn friction on stress concentration near yarn breaks in woven fabrics. Text Res J 73:292–304
31. Roylance D, Wang SS (1980) Penetration mechanics of textile structures, ballistic materials and penetration mechanics. Elsevier, Amsterdam, pp 273–293
32. Sacks MS, Sun W (2003) Multiaxial mechanical behavior of biological materials. Annu Rev Biomed Eng 5:251–284
33. Shim VP, Tan VBC, Tay TE (1995) Modelling deformation and damage characteristics of woven fabric under small projectile impact. Int J Impact Eng 16:585–605
34. Shockey DA, Erlich DC, Simons JW (2004) Lightweight ballistic protection of flight-critical components on commercial aircraft—large-scale ballistic impact tests and computational simulations. FAA report DOT/FAA/AR-04/45, P2
35. Steigmann DJ (1990) Tension field theory. Proc R Soc Lond A 429:141–173
36. Tabiei A, Jiang Y (1999) Woven fabric composite material model with material nonlinearity for finite element simulation. Int J Solids Struct 36:2757–2771
37. Tabiei A, Nilakantan G (2008) Ballistic impact of dry woven fabric composites: a review. Appl Mech Rev 61:1–13
38. Tan VBC, Shim VPW, Zeng X (2005) Modelling crimp in woven fabrics subjected to ballistic impact. Int J Impact Eng 32:561–574
39. Taylor WJ, Vinson JR (1990) Modelling ballistic impact into flexible materials. AIAA J 28:2098–2103
40. Toyobo (2001) PBO fiber ZYLON. Report of the Toyobo Corporation, LTD. http://www.toyobo.co.jp
41. Verzemnieks J (2005) Lightweight ballistic protection of flight-critical components on commercial aircraft—Zylon Yarn tests. FAA report DOT/FAA/AR-05/45, P3
42. Walker JD (1999) Constitutive model for fabrics with explicit static solution and ballistic limit. In: Proceedings of the 18th international symposium on ballistics, San Antonio, TX, pp 1231–1238
43. Wriggers P (2002) Computational contact mechanics. Wiley, New York
44. Zohdi TI (2002) Modeling and simulation of progressive penetration of multilayered ballistic fabric shielding. Comput Mech 29: 61–67
45. Zohdi TI, Steigmann DJ (2002) The toughening effect of microscopic filament misalignment on macroscopic fabric response. Int J Fract 115:L9–L14
46. Zohdi TI (2004) Modeling and direct simulation of near-field granular flows. Int J Solids Struct 42/2:539–564

47. Zohdi TI (2004) A computational framework for agglomeration in thermo-chemically reacting granular flows. Proc R Soc 460(2052):3421–3445
48. Zohdi TI (2005) Charge-induced clustering in multifield particulate flow. Int J Numer Methods Eng 62(7):870–898
49. Zohdi TI, Powell D (2006) Multiscale construction and large-scale simulation of structural fabric undergoing ballistic impact. Comput Methods Appl Mech Eng 195(1–3):94–109
50. Zohdi TI (2007) Computation of strongly coupled multifield interaction in particle-fluid systems. Comput Methods Appl Mech Eng 196:3927–3950
51. Zohdi TI (2007) A computational framework for network modeling of fibrous biological tissue deformation and rupture. Comput Methods Appl Mech Eng 196:2972–2980
52. Zohdi TI (2007) Introduction to the modeling and simulation of particulate flows. SIAM (Society for Industrial and Applied Mathematics)
53. Zohdi TI (2009) Mechanistic modeling of swarms. Comput Methods Appl Mech Eng 198(21–26):2039–2051